Pathloss modeling for in-body optical wireless communications

Stylianos E. Trevlakis, Alexandros-Apostolos A. Boulogeorgos, and Nestor D. Chatzidiamantis
Department of Electrical and Computer Engineering, Aristotle University of Thessaloniki, Thessaloniki, Greece, 54124
Emails: {trevlakis; nestoras}@auth.gr; al.boulogeorgos@ieee.org

***Abstract*—Optical wireless communications (OWCs) have been recognized as a candidate enabler of next generation in-body nano-scale networks and implants. The development of an accurate channel model capable of accommodating the particularities of different type of tissues is expected to boost the design of optimized communication protocols for such applications. Motivated by this, this paper focuses on presenting a general pathloss model for in-body OWCs. In particular, we use experimental measurements in order to extract analytical expressions for the absorption coefficients of the five main tissues' constitutions, namely oxygenated and de-oxygenated blood, water, fat, and melanin. Building upon these expressions, we derive a general formula for the absorption coefficient evaluation of any biological tissue. To verify the validity of this formula, we compute the absorption coefficient of complex tissues and compare them against respective experimental results reported by independent research works. Interestingly, we observe that the analytical formula has high accuracy and is capable of modeling the pathloss and, therefore, the penetration depth in complex tissues.**

***Index Terms*—Absorption coefficient, biomedical engineering, fitting, machine learning, optical properties.**

I. Introduction

Optical wireless communication (OWC) based in-body biomedical applications have attracted a significant amount of attention over the last couple of years, due to the performance excellency (in terms of reliability, speed, energy efficiency and latency) that they are expected to achieve [1]–[6]. In order to optimize the in-body OWC system performance, an accurate channel model that takes into account the tissue characteristics needs to be employed.

Scanning the technical literature, it can be observed that most efforts focus on quantifying the optical characteristics of specific tissues at certain wavelengths [7]–[17]. Also, in [7]–[9], the authors performed measurements for the optical properties of both healthy and cancerous skin in the visible and near-infrared spectral range. In [10]–[12], experiments were performed that quantified the optical properties of human female breast tissues in multiple wavelengths and over different distances. Furthermore, the authors in [13], [14] evaluated the light absorption and scattering of bone tissue for various wavelengths in the visible and near-infrared spectrum. Finally, in [15]–[17], the optical properties of human brain tissue at various ages were studied in the visible spectrum. However, such results are not always useful for other researchers due to various reasons. Firstly, they may not include the required wavelengths of interest. Secondly, even if the wavelength is available, the constitution of a tissue is different enough between distinct individuals that the results cannot be regarded as confident. As a result, the need arises for the development of method that estimates the optical properties of a tissue based on its constitution.

To this end, specific formulas have been reported for the pathloss evaluation of a generic tissue that take into account the variable amounts of its constituents (i.e. blood, water, fat, melanin), but require their optical properties at the exact transmission wavelength, which hinders the use of these formulas [18], [19]. Motivated by this, this paper derives a novel mathematical model, which requires no experimental measurements for the calculation of the pathloss for in-body OWCs. Based on the aforementioned, the technical contribution of the this work is summarized as follows:

- We extract analytical expressions for the absorption coefficients of the five main tissues' constitutions, namely oxygenated and de-oxygenated blood, water, fat, and melanin.
- Based on the these expressions, we derive a general formula for the absorption coefficient evaluation of any biological tissue.
- We present the analytical results for the absorption coefficients of complex human tissues, such as brain, bone, breast and skin, and compare them with experimental results reported by independent works that prove the validity of the presented mathematical framework.
- Finally, we illustrate the pathloss as a function of the transmission wavelength for different complex tissues and tissue thickness, and provide discussions that highlight useful insights for the design of communication protocols.

The rest of this paper is organized as follows. Section II is devoted in presenting the pathloss model based on the absorption properties of the constituents of any generic tissue. Section III presents respective numerical results that verify the mathematical framework and insightful discussions, which highlight design guidelines for communication protocols. Finally, closing remarks are summarized in Section IV.

Notations: Unless stated otherwise, in this paper, $\exp(\cdot)$ represents the exponential function, while $\cos(\cdot)$ and $\sin(\cdot)$ stand for the cosine and sine functions, respectively.

II. Pathloss Model

The pathloss caused by the absorption of biological tissue can be modeled as

$$L = \exp\left(\mu_a \delta\right), \tag{1}$$

where δ is the transmission distance and μ_a is the absorption coefficient, which can be defined as

$$\mu_a = -\frac{1}{T}\frac{\partial T}{\partial \delta}, \tag{2}$$

with T denoting the fraction of residual optical radiation at δ. Thus, the fractional change of the intensity of the incident light can be obtained as

$$T = \exp\left(-\mu_a \delta\right). \tag{3}$$

The absorption coefficient can be expressed as the sum of all the tissue's constituents, namely water, melanin, fat, oxygenated blood and de-oxygenated blood. Thus, (2) can be analytically expressed as in [18]

$$\begin{aligned}\mu_a =& BS\mu_{a(oBl)} + B\left(1-S\right)\mu_{a(dBl)} \\ &+ W\mu_{a_{(w)}} + F\mu_{a_{(f)}} + M\mu_{a_{(m)}}\end{aligned}, \tag{4}$$

where $\mu_{a(i)}$ represents the absorption coefficient of the i-th constituent, while B, W, F, and M represent the blood, water, fat, and melanin volume fractions, respectively. Finally, S denotes the oxygen saturation of hemoglobin.

From (4), it becomes evident that, in order to evaluate the absorption coefficients and volume fractions of each constituent in order to calculate the complete absorption coefficient of any tissue. Although the techniques for measuring optical properties evolve in terms of accuracy and speed, the fact that tissue's optical properties must be regarded as variables between different tissues, people and even times, hinders their mathematical modeling. These variations, on the one hand are inherent on the individuality of each person, while on the other hand they are subject to the measurement techniques and tissue preparation protocols. However, the absorption coefficients of the tissue's constituents have been measured in existing literature and are mainly dependent on the wavelength of the transmitted optical radiation.

In this direction, we used the machine learning mechanism based on non-linear regression, which is presented in Fig.1, to extract analytical expressions for the absorption coefficients of oxygenated and de-oxygenated blood, water, fat, and melanin from on the experimental datasets for each of the constituents as input [20]. In particular, absorption coefficient datasets of oxygenated and de-oxygenated blood have been provided in [21]–[24]. The analytical expressions of the absorption coefficients of oxygenated and de-oxygenated blood, have been fitted on the experimental results using the sum of Gaussian functions and can be expressed as

$$\mu_{a(dBl)}\left(\lambda\right) = \sum_{i=1}^{4} a_{i(dBl)} \exp\left(-\left(\frac{\lambda - b_{i(dBl)}}{c_{i(dBl)}}\right)^2\right), \tag{5}$$

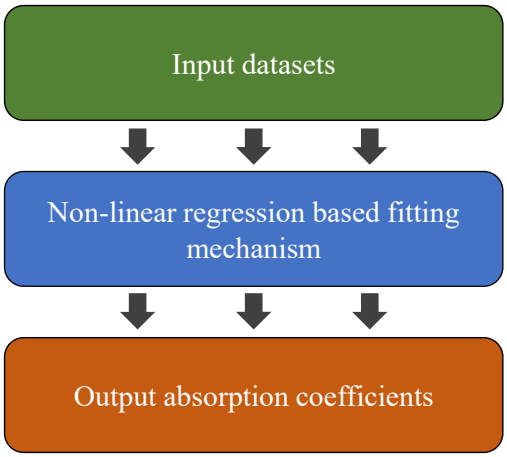

Fig. 1. Machine learning based fitting mechanism.

and

$$\mu_{a(oBl)}\left(\lambda\right) = \sum_{i=1}^{5} a_{i(oBl)} \exp\left(-\left(\frac{\lambda - b_{i(oBl)}}{c_{i(oBl)}}\right)^2\right). \tag{6}$$

Furthermore, the absorption coefficient of water has been evaluated in several contributions [25]–[27], which were used to extract a Fourier series that accurately describes the absorption coefficient as a function of the transmission wavelength. The extracted analytical expression of the absorption coefficient of water can be written as

$$\mu_{a_{(w)}}\left(\lambda\right) = a_{0_{(w)}} + \sum_{i=1}^{7} a_{i_{(w)}} \cos(iw\lambda) + b_{i_{(w)}} \sin(iw\lambda). \tag{7}$$

Moreover, the absorption of fat is highly dependent on the origin of the fat. For proper measurement of the optical properties, the fat tissue must be purified and dehydrated. This necessary preparation may cause inconsistencies between different published works. However, the results presented in [28] coincide with other works in the visible spectrum and, thus, they are selected for extracting the mathematical model for the absorption coefficient of fat. The analytical expression was extracted by fitting the experimental measurements with a sum of Gaussian functions and is given by

$$\mu_{a(f)}\left(\lambda\right) = \sum_{i=1}^{5} a_{i(f)} \exp\left(-\left(\frac{\lambda - b_{i(f)}}{c_{i(f)}}\right)^2\right). \tag{8}$$

It should be highlighted that the parameters of the previously extracted analytical expressions are provided in Table I. Finally, the experimental data available in open literature for the absorption coefficient of melanin are highly consistent for the visible spectrum [18], [29], [30]. Based on these results, the analytical expression of the absorption coefficient of melanin is given as

$$\mu_{a_{(m)}}\left(\lambda\right) = \mu_{a_{(m)}}\left(550\right)\left(\frac{\lambda}{550}\right)^{-3}, \tag{9}$$

TABLE I
FITTING PARAMETERS FOR CONSTITUENT'S ABSORPTION COEFFICIENT.

	dBlood	oBlood	water	fat
a_0	-	-	324.1	-
a_1	38.63	14	102.2	33.53
a_2	60.18	13.75	-568	50.09
a_3	25.11	29.69	-126.6	3.66
a_4	2.988	4.317×10^{15}	236.8	2.5
a_5	-	-34.3	73	19.86
a_6	-	-	-40.53	-
a_7	-	-	-12.92	-
b_1	423.9	419.7	697.9	411.5
b_2	31.57	581.5	121.7	968.7
b_3	559.3	559.9	-395.3	742.9
b_4	664.7	-25880	-107.1	671.2
b_5	-	642.6	115.6	513.8
b_6	-	-	35.46	-
b_7	-	-	-8.373	-
c_1	33.06	16.97	-	38.38
c_2	660.8	11.68	-	525.9
c_3	59.08	46.71	-	80.22
c_4	28.53	4668	-	32.97
c_5	-	162.5	-	119.2
w	-	-	0.006663	-

where $\mu_{a_{(m)}}(550)$ denotes the absorption coefficient of melanin at 550 nm, which is equal to 519 cm^{-1}.

III. RESULTS & DISCUSSION

This section focuses not only on the verification of the mathematical framework presented in Section II via comparing the experimental data with the analytical expressions derived from it, but also on the illustration of its accuracy in modeling complex biological tissues, such as skin, bone, breast, and brain tissue. Finally, the pathloss is evaluated for each complex tissue and insightful discussions are provided that illustrates important design guidelines for communication protocols.

Fig. 2 depicts the experimental data for each constituent's absorption coefficient against the analytical results extracted from (6) through (9). In more detail, the analytical expressions for the oxygenated and de-oxygenated blood, water, melanin, and fat are drawn in black, red, green, blue, and purple color, respectively, while the corresponding experimental data are represented by square, circle, star, triangle, and cross symbols. The analytical and experimental results coincide, which proves the validity of the analytical expressions. Another interesting observation from this figure is that the absorption coefficient of blood is higher than the rest constituents between 400 and 600 nm, while it is still among the most influential for higher wavelength values. This highlights that even with relatively low volume fraction, blood plays an important role in the total absorption coefficient of any generic tissue. Furthermore, it is evident that as λ increases, the absorption coefficient increases as well, which highlights the importance of carefully

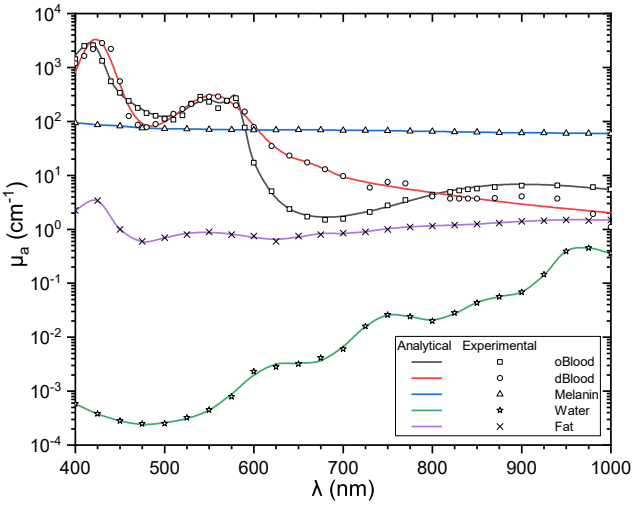

Fig. 2. Absorption coefficients of generic tissue constituents as a function of the transmission wavelength.

selecting the transmission wavelength used in tissues with high concentration in water. Moreover, we observe that the absorption coefficient of fat receives values around 1 cm^{-1} with very small variations, which constitutes its impact on the total absorption of generic tissues stable throughout the visible spectrum. Finally, it becomes evident that the absorption of melanin is among the highest between the generic tissue constituents, but the most consistent throughout the visible spectrum. This illustrates the importance of the concentration of melanin in the tissue under investigation and, at the same time, the negligible effect of the transmission wavelength on the absorption due to melanin.

It should be highlighted that, the volume fraction of any of the constituents plays a very important role in the final form of the absorption coefficient. For example, if a tissue is rich in water, the impact of the absorption coefficient of water after it is multiplied by the water volume fraction can affect the total absorption coefficient significantly, even if the absorption coefficient of water seems insignificant on its own. On the other hand, the impact of a constituent with high absorption coefficient, such as melanin, can be diminished if it has a low volume fraction. As a result, although the absorption coefficients presented in Fig. 2 are very useful for determining which constituents can affect the total absorption coefficient of the generic tissue, it is not an absolute metric and must be used with caution for making assumptions. In the rest of this section, we present experimental results from the open literature for the absorption coefficients of complex human tissues and compare them to the estimation calculated based on the mathematical framework that is presented above.

In Fig. 3, the absorption coefficients of complex tissues, such as skin, bone, brain and breast, are presented as a function of the transmission wavelength. The analytical expressions and the experimental results are depicted as continuous lines and circles, respectively. The experimental parameters for each tissue are provided in Table II alongside their sources.

TABLE II
TISSUE PARAMETERS RELATED TO OPTICAL ABSORPTION FOR SKIN, BONE, BRAIN AND BREAST TISSUE.

Tissue	$B(\%)$	$S(\%)$	$W(\%)$	$F(\%)$	$M(\%)$	Source
Skin	0.41	99.2	26.1	22.5	1.15	[7]–[10]
Breast	0.5	52	50	13	0	[10]–[12]
Bone	0.15	30	30	7	0	[10], [13], [14]
Brain	1.71	58.7	50	20	0	[15]–[17]

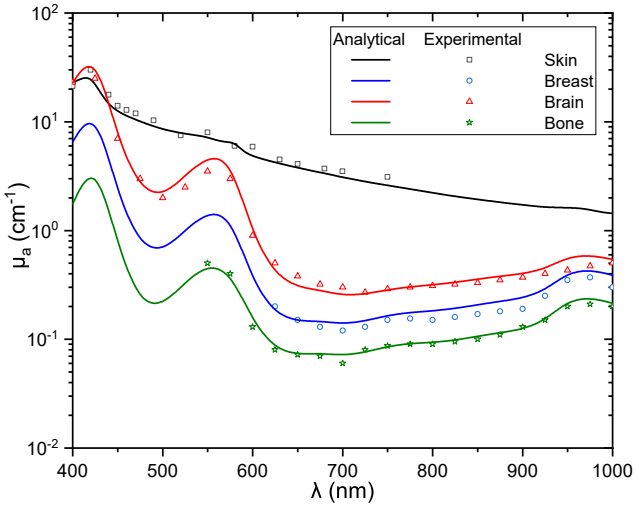

Fig. 3. Total absorption coefficient of complex tissues as a function of the transmission wavelength.

From this figure, we observe that the analytical expression for the total absorption coefficient provides a very close fit to the experimental data, which verifies the validity of the extracted expressions and provides proof that the presented mathematical framework can describe the optical absorption of generic tissues accurately. Furthermore, it is obvious that the skin absorption coefficient has the most linear behavior out of all the plotted tissues. This happens because of the increased concentration of melanin in the skin, which leads to increased absorption for higher wavelengths. On the other hand, the absorption coefficients of other tissues, which have increased blood and water concentrations, bare a strong resemblance to the blood absorption coefficient in the region between 400 and 600 nm, while the impact of the absorption coefficient of water becomes visible after 900 nm. This happens because the higher blood and water volume fractions result in increased absorption in the wavelengths where each absorption coefficient has relatively high values.

Having extracted the accurate absorption coefficients for the various complex tissues, we can calculate the pathloss. To this end, Fig. 4 depicts the pathloss as a function of the wavelength due to absorption in skin tissues with different values of thickness. By observing this figure, it becomes evident that the pathloss decreases with the wavelength and increases with the skin thickness. Thus, the optimal wavelength in the plotted region is 1000 nm. Furthermore, in the following we assume

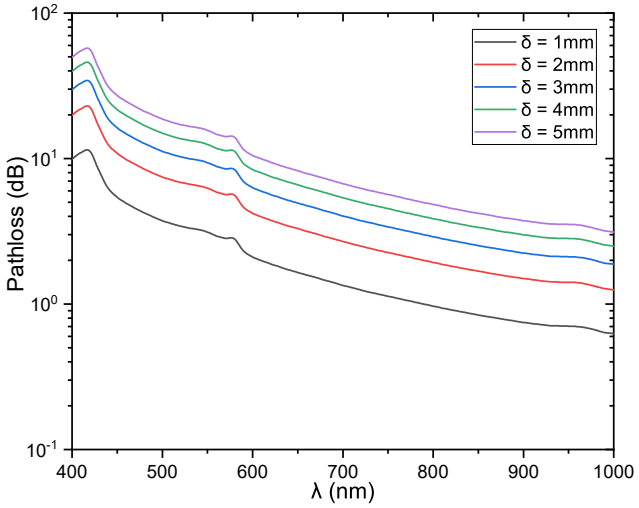

Fig. 4. Pathloss due to skin absorption as a function of the transmission wavelength for different values of skin thickness.

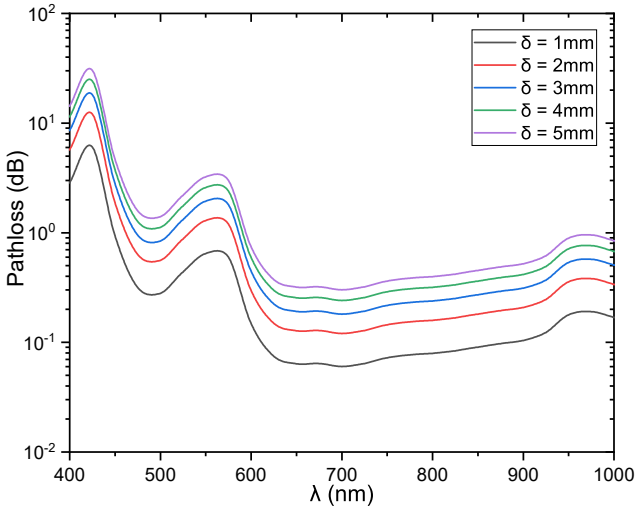

Fig. 5. Pathloss due to breast absorption as a function of the transmission wavelength for different values of breast thickness.

a transmission window to be the spectrum region where the pathloss does not exceed 6 dB, i.e. the residual optical signal is at least a quarter of the transmitted one. Thus, for $\delta = 1$ mm a transmission window exists for wavelength values higher than 450 nm. However, this transmission windows shrinks as the transmission distance increases. For example, for $\delta = 3$ mm it reduces to wavelengths higher than 650 nm, while for $\delta = 3$ mm it becomes even smaller for wavelengths higher than 650 nm.

In Fig. 5, the pathloss of breast tissue is presented with regard to the transmission wavelength for various values of transmission distance. We observe that, as the δ increases, the pathloss increases as well. On the contrary, the wavelength influences the pathloss in a non linear manner. Moreover, a single transmission window exists for all the plotted values of δ and is located after 550 nm. However, for higher values of

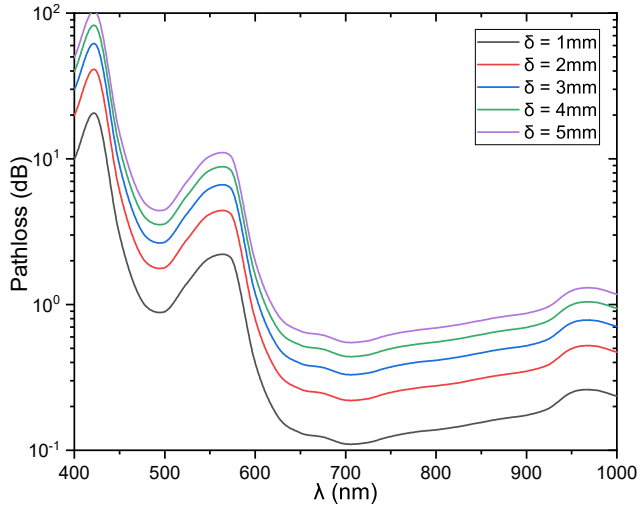

Fig. 6. Pathloss due to brain absorption as a function of the transmission wavelength for different values of brain thickness.

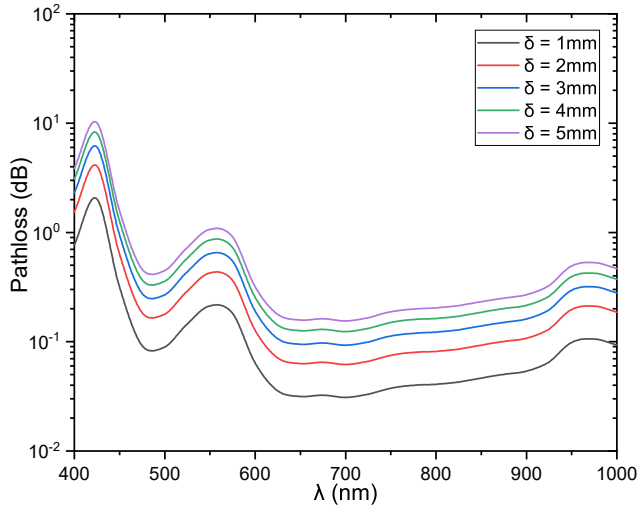

Fig. 7. Pathloss due to bone absorption as a function of the transmission wavelength for different values of bone thickness.

δ this transmission window will be divided in two. Finally the optimal transmission wavelength for breast tissue is 700 nm.

Fig. 6 illustrates the pathloss as a function of the wavelength for different values of tissue thickness. As expected, for higher values of δ the pathloss is also higher, while the behavior of pathloss for wavelength variations is not linear. For example, as λ increases from 500 to 550 nm the pathloss increases, while for the same increase from 550 to 600 nm, pathloss decreases. Also, the optimal transmission wavelength is 700 nm. Furthermore, two transmission windows exist for $\delta = 1$ mm. The first is between 450 and 550 nm, while the second after 600 nm. However, as the transmission distance increases, only the second window will be valid.

In Fig. 7, the pathloss is depicted as a function of the transmission wavelength for various transmission distance values. Yet again, pathloss increases with tissue thickness, while its behavior with regard to λ changes depends. The optimal λ for transmission through bone tissue is 700 nm. For δ equal to 1 and 2 mm, only one transmission window exists for λ higher than 450 nm. On the contrary, for higher δ values, there are two transmission windows. For example, for $\delta = 5$ mm, the two windows are $475 - 525$ nm, and $600 - 950$ nm.

IV. Conclusion

In this paper, we first extracted analytical expressions for the absorption coefficient of the major generic tissue constituents based on published experimental measurements. These expressions enable the estimation of the absorption coefficient of each constituent at any given wavelength. Based on them, we formulate the mathematical framework for calculating the absorption coefficient of any generic tissue with regard to the transmission wavelength. Finally, we present the analytical results for the absorption coefficients of complex human tissues, compare them with experimental results from the open literature that prove the validity of the presented mathematical framework. Finally, we illustrate the pathloss as a function of the transmission wavelength for different complex tissues and tissue thickness, and provide insightful discussions.

Aknowledgement

This research is co-financed by Greece and the European Union (European Social Fund-ESF) through the Operational Programme "Human Resources Development, Education and Lifelong Learning 2014-2020" in the context of the project "IRIDA-Optical wireless communications for in-body and transdermal biomedical applications" (MIS 5047929).

References

[1] S. E. Trevlakis, A.-A. A. Boulogeorgos, and G. K. Karagiannidis, "On the impact of misalignment fading in transdermal optical wireless communications," in *7th International Conference on Modern Circuits and Systems Technologies (MOCAST)*, May 2018.

[2] S. Trevlakis, A.-A. A. Boulogeorgos, and G. Karagiannidis, "Signal quality assessment for transdermal optical wireless communications under pointing errors," *Technologies*, vol. 6, no. 4, p. 109, Nov. 2018.

[3] S. E. Trevlakis, A.-A. A. Boulogeorgos, and G. K. Karagiannidis, "Outage performance of transdermal optical wireless links in the presence of pointing errors," in *IEEE 19th International Workshop on Signal Processing Advances in Wireless Communications (SPAWC)*, Jun. 2018.

[4] S. E. Trevlakis, A.-A. A. Boulogeorgos, P. C. Sofotasios, S. Muhaidat, and G. K. Karagiannidis, "Optical wireless cochlear implants," *Biomedical Optics Express*, vol. 10, no. 2, p. 707, Jan. 2019.

[5] S. E. Trevlakis, A.-A. A. Boulogeorgos, N. D. Chatzidiamantis, and G. K. Karagiannidis, "All-optical cochlear implants," *IEEE Trans. Mol. Biol. Multi-Scale Commun.*, vol. 6, no. 1, pp. 13–24, Jun. 2020.

[6] A.-A. A. Boulogeorgos, S. E. Trevlakis, and N. D. Chatzidiamantis, "Optical wireless communications for in-body and transdermal biomedical applications," *IEEE Commun. Mag.*, Jan. 2021.

[7] T.-Y. Tseng, C.-Y. Chen, Y.-S. Li, and K.-B. Sung, "Quantification of the optical properties of two-layered turbid media by simultaneously analyzing the spectral and spatial information of steady-state diffuse reflectance spectroscopy," *Biomed. Opt. Express*, vol. 2, no. 4, p. 901, Mar. 2011.

[8] E. Salomatina, B. Jiang, J. Novak, and A. N. Yaroslavsky, "Optical properties of normal and cancerous human skin in the visible and near-infrared spectral range," *J. Biomed. Opt.*, vol. 11, no. 6, p. 064026, Nov. 2006.

[9] Y. Shimojo, T. Nishimura, H. Hazama, T. Ozawa, and K. Awazu, "Measurement of absorption and reduced scattering coefficients in asian human epidermis, dermis, and subcutaneous fat tissues in the 400- to 1100-nm wavelength range for optical penetration depth and energy deposition analysis," *J. Biomed. Opt.*, vol. 25, no. 04, p. 1, Apr. 2020.

[10] J. L. Sandell and T. C. Zhu, "A review of in-vivo optical properties of human tissues and its impact on PDT," *J. Biophotonics*, vol. 4, no. 11-12, pp. 773–787, Oct. 2011.

[11] A. Pifferi, J. Swartling, E. Chikoidze, A. Torricelli, P. Taroni, A. Bassi, S. Andersson-Engels, and R. Cubeddu, "Spectroscopic time-resolved diffuse reflectance and transmittance measurements of the female breast at different interfiber distances," *J. Biomed. Opt.*, vol. 9, no. 6, p. 1143, Nov. 2004.

[12] L. Spinelli, A. Torricelli, A. Pifferi, P. Taroni, G. M. Danesini, and R. Cubeddu, "Bulk optical properties and tissue components in the female breast from multiwavelength time-resolved optical mammography," *J. Biomed. Opt.*, vol. 9, no. 6, p. 1137, Nov. 2004.

[13] A. N. Bashkatov, E. A. Genina, V. I. Kochubey, and V. V. Tuchin, "Optical properties of human cranial bone in the spectral range from 800 to 2000 nm," in *Saratov Fall Meeting 2005: Optical Technologies in Biophysics and Medicine VII*, V. V. Tuchin, Ed. SPIE, Aug. 2006.

[14] N. Ugryumova, S. J. Matcher, and D. P. Attenburrow, "Measurement of bone mineral density via light scattering," *Phys. Med. Biol.*, vol. 49, no. 3, pp. 469–483, Jan. 2004.

[15] J. Zhao, H. S. Ding, X. L. Hou, C. L. Zhou, and B. Chance, "In vivo determination of the optical properties of infant brain using frequency-domain near-infrared spectroscopy," *J. Biomed. Opt.*, vol. 10, no. 2, p. 024028, Mar. 2005.

[16] A. N. Yaroslavsky, P. C. Schulze, I. V. Yaroslavsky, R. Schober, F. Ulrich, and H.-J. Schwarzmaier, "Optical properties of selected native and coagulated human brain tissues in vitro in the visible and near infrared spectral range," *Phys. Med. Biol.*, vol. 47, no. 12, pp. 2059–2073, Jun. 2002.

[17] P. van der Zee, M. Essenpreis, and D. T. Delpy, "Optical properties of brain tissue," in *Photon Migration and Imaging in Random Media and Tissues*, B. Chance and R. R. Alfano, Eds. SPIE, Sep. 1993.

[18] S. L. Jacques, "Optical properties of biological tissues: a review," *Phys. Med. Biol.*, vol. 58, no. 11, pp. R37–R61, May 2013.

[19] S. E. Trevlakis, A. A. A. Boulogeorgos, N. D. Chatzidiamantis, G. K. Karagiannidis, and X. Lei, "Electrical vs optical cell stimulation: A communication perspective," vol. 8, pp. 192 259–192 269.

[20] A.-A. A. Boulogeorgos, S. E. Trevlakis, S. A. Tegos, V. K. Papanikolaou, and G. K. Karagiannidis, "Machine learning in nano-scale biomedical engineering."

[21] S. Takatani and M. D. Graham, "Theoretical analysis of diffuse reflectance from a two-layer tissue model," *IEEE. Trans. Biomed. Eng.*, vol. BME-26, no. 12, pp. 656–664, Dec. 1979.

[22] M. K. Moaveni, *A multiple scattering field-theory applied to whole blood*. Univ. of Washington, 1970.

[23] J. Schmitt, *Optical Measurement of Blood Oxygen by Implantable Telemetry*. Stanford University, 1986. [Online]. Available: https://books.google.gr/books?id=jIgPIQAACAAJ

[24] Y. Zhao, L. Qiu, Y. Sun, C. Huang, and T. Li, "Optimal hemoglobin extinction coefficient data set for near-infrared spectroscopy," *Biomed. Opt. Express*, vol. 8, no. 11, p. 5151, Oct. 2017.

[25] G. M. Hale and M. R. Querry, "Optical constants of water in the 200-nm to 200-μm wavelength region," *Appl. Opt.*, vol. 12, no. 3, p. 555, Mar. 1973.

[26] V. M. Zolotarev, B. A. Mikhailov, L. I. Alperovich, and S. I. Popov, "Dispersion and Absorption of Liquid Water in the Infrared and Radio Regions of the Spectrum," *Opt. Spectrosc.*, vol. 27, p. 430, Nov. 1969.

[27] D. J. Segelstein, "The complex refractive index of water," Ph.D. dissertation, University of Missouri–Kansas City, 1981.

[28] A. N. Bashkatov, "Optical properties of the subcutaneous adipose tissue in the spectral range 400–2500 nm," *Opt. Spectrosc.*, vol. 99, no. 5, p. 836, Nov. 2005.

[29] S. L. Jacques and D. J. McAuliffe, "The melanosome: threshold temperature for explosive vaporization and internal absorption coefficient during pulsed laser irradiation." *Photochem. Photobiol.*, vol. 53, no. 6, pp. 769–775, Jun. 1991.

[30] G. Zonios, A. Dimou, I. Bassukas, D. Galaris, A. Tsolakidis, and E. Kaxiras, "Melanin absorption spectroscopy: new method for non-invasive skin investigation and melanoma detection," *J. Biomed. Opt.*, vol. 13, no. 1, p. 014017, Jan. 2008.